Sustainable Energy & Fuels

ROYAL SOCIETY OF CHEMISTRY

PAPER

View Article Online
View Journal | View Issue

Cite this: *Sustainable Energy Fuels*, 2024, **8**, 4324

Dopant-free fluorene based dimers linked with thiophene units as prospective hole transport materials for Sb_2S_3 solar cells†

Nimish Juneja, [a] Aistė Jegorovė, [b] Raitis Grzibovskis, [c] Atanas Katerski, [a] Maryte Daskeviciene, [b] Tadas Malinauskas, [b] Aivars Vembris, [c] Smagul Karazhanov, [d] Nicolae Spalatu, [a] Vytautas Getautis, [b] Malle Krunks *[a] and Ilona Oja Acik [a]

Novel dopant-free dimers comprising methoxydiphenylamine substituted fluorene derivatives and connected by central cores consisting of different numbers of thiophene moieties were synthesized and explored as hole transport materials (HTMs) in Sb_2S_3 absorber solar cells. Energy level diagrams show agreeable band offsets validating the compatibility of novel HTMs for the FTO/TiO_2/Sb_2S_3/HTM/Au solar cell with TiO_2 and Sb_2S_3 layers deposited by ultrasonic spray. X-ray photoelectron spectroscopy (XPS) study reveals the Sb 3d core level peak shift upon applying any of the HTMs on Sb_2S_3 indicating an increased electron density surrounding Sb atoms which refers to the interaction of S from electron-rich thiophene units with Sb in the absorber at the Sb_2S_3/HTM interface. It is demonstrated that application of HTMs containing diphenylamine units in their side fragments increases the cell open circuit voltage from 478 mV to 673 mV, fill factor from 46% to 56% and conversion efficiency from 1.9% to 4.5% as compared to the device without any HTM and the observed improvement can be explained by the passivation of the interfacial states. In contrast, no enhancement in device performance has been observed when applying HTMs containing triphenylamine units although strong Sb–S interaction has been detected at the Sb_2S_3/HTM interface. Quantum chemical simulation results suggest that to achieve enhanced charge selectivity by the organic HTM layer, the HOMO of the HTMs should be formed by the thiophene groups. Possible phenomena occurring at the Sb_2S_3/HTM interface are discussed providing new insights towards understanding the charge transfer at the Sb_2S_3/HTM interface.

Received 8th April 2024
Accepted 16th July 2024

DOI: 10.1039/d4se00472h

rsc.li/sustainable-energy

1. Introduction

The need for resource saving energy applications in society requires accelerated development and design of materials and solar cell devices with a wide set of properties which would allow an extended application range beyond Si photovoltaics (PVs). At this scale, for a new PV technology, it is insufficient to be only competitive with the current established c-Si or CdTe thin film technologies regarding the performance and stability but it should also be environmentally friendly and comprise earth abundant chemical elements. An emerging family of promising cost-efficient PV materials, such as antimony and bismuth-based chalcogenides[1–3] and lead-free chalcogenide perovskites[4] are currently under investigation in the PV community. Among these materials, antimony chalcogenides such as Sb_2S_3, Sb_2Se_3 and $Sb_2(S,Se)_3$ showed a nascent track record of rapid performance development, reaching power conversion efficiencies (PCEs) of 8.0%, 10.57% and 10.75%, respectively.[5–7] These materials have garnered substantial R&D efforts within the PV community due to their compelling attributes such as their abundance in nature, environmentally benign elemental constituents, as well as commendable optoelectronic characteristics and stability.[2,8,9] In particular, the utility of Sb_2S_3 absorbers makes them viable for employment in semi-transparent solar cells, owing to their band gap of 1.7 eV, and a high absorption coefficient (10^5 cm^{-1} at 450 nm). These advantageous attributes make them particularly well-suited for integration within tandem cell device configurations and as solar windows.

In many solar cells, including antimony chalcogenide-based solar cells, a hole transporting layer (HTL) is utilized to extract and transport photogenerated charge carriers from the

[a]*Department of Materials and Environmental Technology, Tallinn University of Technology, Ehitajate tee 5, Tallinn, 19086, Estonia. E-mail: malle.krunks@ttu.ee*
[b]*Department of Organic Chemistry, Kaunas University of Technology, Kaunas, LT-50254, Lithuania*
[c]*Institute of Solid State Physics, University of Latvia, Kengaraga Str. 8, Riga, LV-1063, Latvia*
[d]*Institute for Energy Technology (IFE), P.O. Box 40, Kjeller, NO 2027, Norway*

† Electronic supplementary information (ESI) available. See DOI: https://doi.org/10.1039/d4se00472h

absorber layer to the electrode. The HTL also serves as a barrier layer for electron leakage and as a protective layer to screen the active layer from oxygen and moisture. The HTL can be made of inorganic and organic materials. An ideal material for the HTL should have an excess of holes, high hole mobility, good thermal stability, low density of defects, high solubility in a suitable solvent, simple synthesis process and appropriate band energy alignment with the absorber.[10,11] In general, organic hole transporting materials (HTMs) like poly(3-hexylthiophene) (P3HT)[11–13] and 2,2′,7,7′-tetrakis[*N*,*N*-di(4-methoxyphenyl)amino]-9,9′-spirobifluorene (Spiro-OMeTAD)[5,14,15] or a combination of them[16] are the most commonly employed to fabricate efficient Sb chalcogenide solar cells, although Spiro-OMeTAD is the most efficient one to date delivering a PCE of around 10%.[7,17,18] However, both these HTMs possess serious drawbacks for large-scale applications. P3HT and Spiro-OMeTAD are expensive due to their complex and time-consuming synthesis processes.[19] In addition, P3HT exhibits parasitic absorption of light in the visible spectral region, leading to a decrease in the overall optical transmittance of the solar cell[13,20–22] while Spiro-OMeTAD exhibits low values of conductivity and hole mobility.[23] Common additives such as lithium bis(trifluoromethanesulfonyl)imide (LiTFSI) and 4-*tert*-butylpyridine (TBP) are used to improve the electrical properties of Spiro-OMeTAD films,[24] which, in turn, seriously worsen the stability of the devices. Therefore, the exploration and advancement of easily synthesizable and dopant-free HTMs is a challenging task.

It has been demonstrated that fluorene-based enamines synthesized by a facile condensation reaction are efficient dopant-free HTMs for high performance perovskite solar cells yielding a PCE of 17.1% that outperforms the device with undoped Spiro-OMeTAD exhibiting a PCE of 10.4%.[25] Fluorene-based enamines were recently explored as dopant-free HTMs in Sb_2S_3 solar cells.[20,21] The devices with new transparent HTMs exhibited higher PCEs, up to 4.3% compared to 3.8% by the reference device with P3HT, and *ca.* 20% higher optical transparency.[21]

Novel transparent HTM molecules comprising 4,4′-dimethoxydiphenylamine-substituted fluorene fragments, widely used in organic HTMs, including Spiro-OMeTAD,[26] and thiophene units mimicking P3HT, were synthesized by a simple and high yield synthesis process.[22] Thiophene units were added into the molecule targeting application in antimony chalcogenide active layer solar cells, as the thiophene could interact with Sb atoms at the absorber/HTM interface and an improvement in interfacial properties is expected.[27–29] In our previous study, HTMs from fluorene-based molecules with terminated thiophene units proved their applicability in Sb_2S_3 solar cells, the devices demonstrate PCEs of 4.7–4.9% and an average optical transparency in the visible spectral range of *ca.* 30%, outperforming the parameters of the P3HT-based device.[22]

In this study four new dopant-free HTMs (V1422, V1423, V1454 and V1455) were synthesized, characterized and explored in Sb_2S_3 solar cells. The novelty of the study lies in development and optimization of new HTMs and their evaluation as prospective charge transport materials in Sb_2S_3 thin film devices. The synthesized molecules are dimers containing diphenylamine units (V1422 and V1423) and triphenylamine units (V1454 and V1455) in their side fragments. The common structural feature of all molecules is that the central core consists of different numbers of thiophene moieties. The properties of the novel HTMs are thoroughly studied; quantum chemical calculations are employed to analyze HTM molecular geometry and determine the Highest Occupied Molecular Orbital (HOMO) and Lowest Unoccupied Molecular Orbital (LUMO) positions. The suitability of the synthesized materials as HTMs in planar Sb_2S_3-based solar cells is examined. The solar cell stack comprises glass/FTO/TiO_2/Sb_2S_3/HTM/Au, with TiO_2 and the absorber layer deposited through ultrasonic spray deposition and the HTM layer *via* spin coating. Various characterization methods applied to the materials, interfaces and devices provide insights on the functionality of this new family of dopant-free HTMs for Sb-chalcogenide-based solar cells.

2. Experimental

2.1. Materials

Chemicals required for the synthesis of the HTMs were purchased from Sigma-Aldrich and TCI Europe and used without any additional purification. Comprehensive information on the synthetic procedures of HTMs is detailed in the ESI.† For the fabrication of solar cells, the following substances were used as received: FTO substrate (10 Ω sq^{-1}), titanium(IV) tetraisopropoxide (TTIP) from Acros Organics (99 wt%), acetylacetone from Acros Organics (99 wt%), ethanol from Estonian Spirit (96.6 vol%), methanol from Sigma-Aldrich (99.9 vol%), antimony trichloride from Sigma-Aldrich (99.99 wt%), thiourea from Sigma-Aldrich (99 wt%), chlorobenzene from Sigma-Aldrich (99.5 vol%), and poly(3-hexylthiophene-2,5-diyl) (P3HT) from Sigma-Aldrich (regio regular, >90%).

2.2. Methods

2.2.1. Fabrication of the solar cell. Solar cell devices are fabricated in superstrate configuration (glass/FTO/TiO_2/Sb_2S_3/HTM/Au) using a similar experimental procedure to that outlined in our previous investigations.[20–22] A fluorine-doped tin oxide (FTO)-coated glass substrate with a sheet resistivity of 10 Ω sq^{-1} is subjected to a cleaning process, with steps involving rinsing and boiling in deionized water, followed by drying with N_2. TiO_2 is deposited using ultrasonic spray pyrolysis (USP) with substrate temperature maintained at 340 °C and then annealed (450 °C, 30 min) on a hot plate in air. Similarly, the absorber Sb_2S_3 is deposited using USP (198 °C) and annealed (250 °C, 5 min) in a N_2 environment. The HTM powders were dissolved in chloro-benzene. The V-series HTM solutions in concentrations of 4, 2, 1 and 0.6 mM were spin-coated (3000 rpm, 30 s) on the absorber at room temperature. For P3HT, 1% wt concentration is utilized, followed by spin coating (3000 rpm, 30 s). The P3HT samples undergo an additional activation step at 170 °C for 5 minutes in a nitrogen environment after spin coating. Subsequently, a thermal evaporation process is employed to deposit

an 80–100 nm thick gold (Au) back contact using a shadow mask (contact area – 7.06 mm^2).

2.2.2. Characterization of synthesized HTMs and fabricated solar cells. Chemical compositions of the synthesised HTMs were studied by NMR and MS spectroscopy. ^1H NMR and ^{13}C NMR spectra were collected at 400 and 101 MHz, respectively on a Bruker Avance III spectrometer. The chemical shifts, expressed in ppm, were relative to tetramethylsilane (TMS). All the experiments were performed at 25 °C. Reactions were monitored by thin-layer chromatography on ALUGRAM SIL G/UV254 plates and developed with UV light. Silica gel (grade 9385, 230–400 mesh, 60 Å, Aldrich) was used for column chromatography. Elemental analysis was performed with an Exeter Analytical CE-440 elemental analyser, Model 440 C/H/N. Thermogravimetric analysis (TGA) was performed on a Q50 thermogravimetric analyser (TA Instruments) at a scan rate of 10 °C min^{-1} under a nitrogen atmosphere. The values are given for a weight-loss of 5% (T_{d5}). Differential scanning calorimetry (DSC) was performed on a TA Instruments Q2000 differential scanning calorimeter under a nitrogen atmosphere. The heating and cooling rate was 10 °C min^{-1}. The UV-vis spectral analysis of the sample in solution (THF, 10^{-4} mol L^{-1}) was performed on a PerkinElmer Lambda 35 UV/VIS spectrophotometer. The layer thickness of the solution is $d = 1$ mm and the diffraction grating crack width is 2 nm.

The ionization potential (I_P) values of all the functional layers were measured by the photoelectron yield spectroscopy (PYS) method. The optical band gap values (E_g) of the absorber and HTM films were calculated from the absorption spectra using Tauc plots. Additionally, the work function of the Au metal contacts was measured through a Kelvin probe. The hole drift mobility of the HTMs was measured utilizing the time-of-flight (ToF) method. The X-ray diffraction (XRD) pattern of the glass/FTO/TiO_2/Sb_2S_3 stack was measured using a Rigaku Ultima-IV with a Cu K_α source ($\lambda = 1.5406$ Å) in the 2θ range of 10–80°. Micro-Raman spectra were measured at room temperature using a Horiba Labram HR 800 instrument. The He–Ne laser intensity was attenuated to 143 mW mm^2 with a focal area of Ø 5 mm. Scanning electron microscopy (SEM) was used to measure the thickness of the absorber and HTM layers. The instrument used was a Zeiss HR FESEM Ultra 55 with an electron beam accelerating voltage of 4 kV.

X-ray photoelectron spectroscopy (XPS) was conducted on a Thermo Fisher ESCALAB Xi system with a monochromatic Al Kα (1486.7 eV) X-ray source, and the studied area had a diameter of 650 μm. The total transmittance and total reflectance spectra of the two cell stacks – glass/HTM and glass/FTO/TiO_2/Sb_2S_3/HTM were recorded on an ultraviolet-visible (UV-VIS) spectrophotometer in the range of 300–1100 nm. The Average Visible Transmittance (AVT) values for the glass/HTM and glass/FTO/TiO_2/Sb_2S_3/HTM samples were calculated from the total transmittance spectra in the range of 400–800 nm. The current–voltage (J–V) characteristics were acquired from a Wavelabs LS-2 LED solar simulator under standard AM1.5G conditions at an irradiance of 100 mW cm^{-2}. The measurements were performed at room temperature. The external quantum efficiency (EQE) spectra were measured using a Newport 69911 system. Density Functional Theory (DFT) calculations were performed using B3LYP functional and the 6-31G(d,p) basis set. The highest occupied and lowest unoccupied molecular orbitals of the molecules were calculated for the optimized molecule geometry of the ground state. All calculations were carried out with the Gaussian 09W program and graphical representation was done using the Avogadro program.[30]

3. Results and discussion

The investigated HTMs can be classified into two distinct groups, as depicted in Fig. 1a: molecules featuring diphenylamine units in their side fragments (V1422 and V1423) and molecules containing triphenylamine units (V1454 and V1455). The common structural feature of both groups is that the central core consists of different numbers of thiophene moieties. The thermal stability of the HTMs was investigated with the help of thermogravimetric analysis (TGA) and differential scanning calorimetry (DSC). The data from TGA suggest that the HTMs decompose in the range of 430–445 °C (Fig. S1, in the ESI†), exceeding the temperature necessary for both the device preparation and operation.[31] Consequently, thiophene linked fluorene-based dimers with a higher molecular mass and therefore stronger intramolecular interaction possess higher decomposition temperatures compared to their monomeric analogues (391–403 °C).[22]

DSC measurements indicate that thiophene linked fluorene-based dimers are molecular glasses, exhibiting glass transition temperatures (T_g) ranging from 148 °C to 175 °C (Fig. S2†), exceeding that of Spiro-OMeTAD (124 °C)[26] as well as of their monomeric analogues.[22] The thermal characteristics of the analysed HTMs are presented in Table 1. Comparing the T_g of new HTMs has revealed that the inclusion of triphenylamine units in HTMs' side fragments (V1454 and V1455) results in an elevated T_g. This increase could be attributed to the higher molecular mass associated with the additional triphenylamine units. It is noteworthy that V1455, with a central trithiophene-based unit and triphenylamine as side fragments, exhibits no endothermic peaks, suggesting an entirely amorphous state (Fig. S2†). This property is advantageous for the formation of homogeneous films, eliminating the potential for film crystallization during either device preparation or operation. The ultraviolet-visible (UV-Vis) absorption spectra of the HTMs (Fig. S3†) present two prominent absorption peaks at wavelengths of 300 and 375 nm, corresponding to the π–π* transitions of the side chromophores. Notably, the spectra exhibit an additional peak in the 425–550 nm range, which corresponds to π–π* transitions, and is attributed to the electron-rich thiophene π systems. Comparison of the absorption curves of molecules featuring diphenylamine units in their side fragments (V1422 and V1423) and molecules containing triphenylamine units (V1454 and V1455) has revealed that the latter show higher absorption. It can be assumed that this is due to the presence of an additional phenyl fragment in these compounds. Moreover, comparison of the absorption spectra presented in Fig. S3† with those reported for monomeric analogues in the previous study[22] revealed that the number and positions of

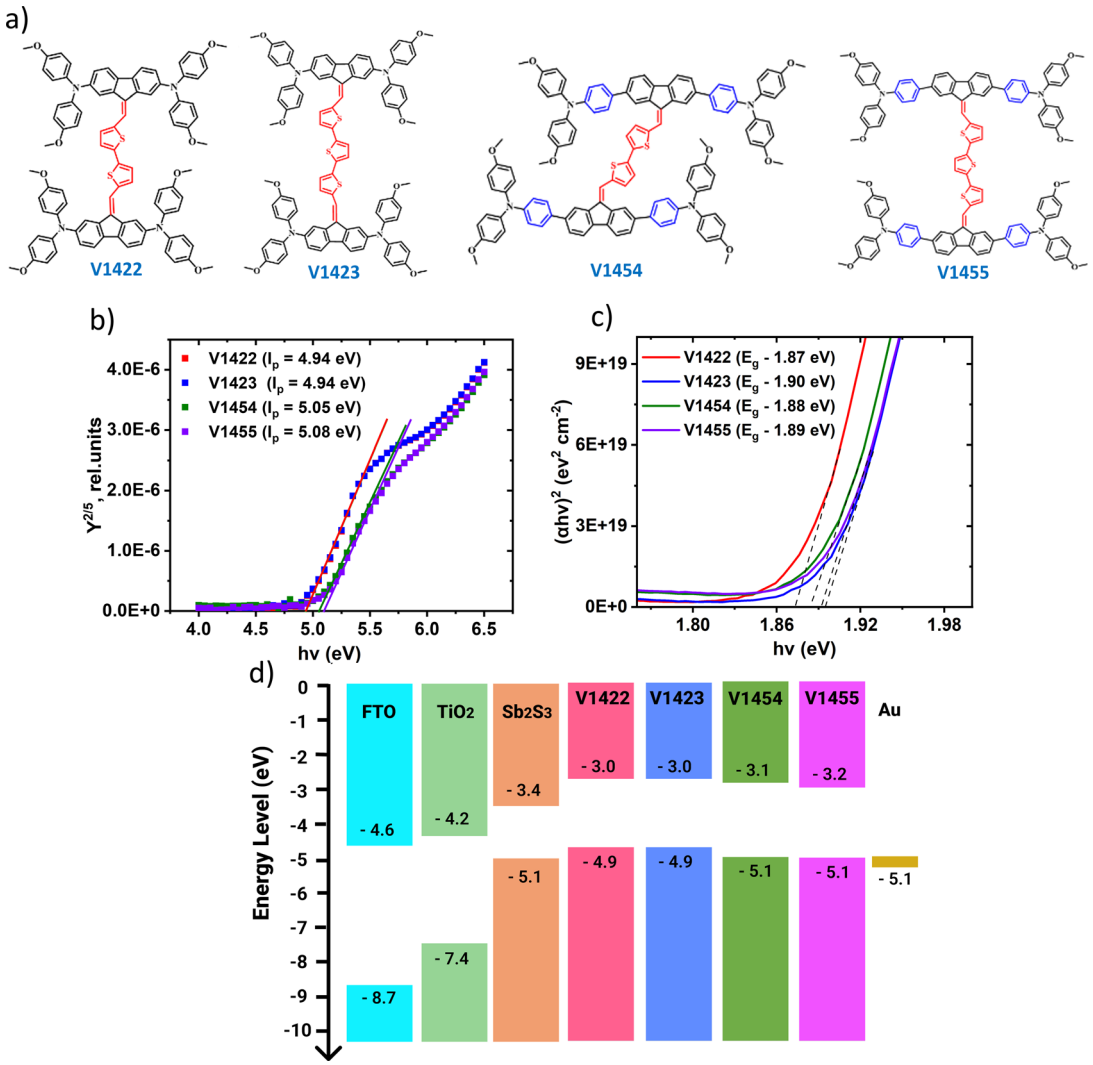

Fig. 1 (a) Chemical structures of synthesised HTMs – V1422, V1423, V1454 and V1455, (b) ionization potential (I_P), and (c) band gap (E_g) values calculated from the absorption spectra using Tauc plots for V1422, V1423, V1454 and V1455 thin films deposited on glass substrates, and (d) energy band diagram of constituent layers of the solar cell.

absorption peaks remain nearly unchanged, indicating that the conjugated system of the thiophene linked fluorene-based dimers is basically unaffected. As presented in Table 1, the inferred zero-field hole mobilities are 9.86×10^{-7}, 1.29×10^{-6}, 3.38×10^{-6}, and 1.85×10^{-6} $cm^2\ V^{-1}\ s^{-1}$ for V1422, V1423, V1454, and V1455, respectively. Therefore, it can be concluded that the presence of the additional phenyl ring in the side diphenyl units of V1454 and V1455 slightly increased the hole drift mobility.

To understand the energy level alignment of the synthesized HTMs with that of Sb_2S_3 and the metal back contact, a Photoelectron Yield Spectroscopy (PYS) technique was employed for measuring the ionization potential (I_P) (see Fig. 1b). The HOMO levels of V1422, V1423, V1454 and V1455 are found to be at −4.94, −4.94, −5.05 and −5.08 eV relative to the vacuum level, respectively. Thus, HTMs bearing triphenylamine units (instead of diphenylamine units) exhibit slightly lower HOMO levels. The calculated band gap (E_g) values for HTMs V1422, V1423,

Table 1 Properties of the synthesized HTMs – V1422, V1423, V1454 and V1455: glass transition temperature (T_g), melting temperature (T_m), 5% weight loss temperature (T_{d5}), optical absorption peak position (λ_{abs}), hole drift mobility (μ_0), band gap energy (E_g) and ionization potential (I_P)

HTM	T_g (°C)	T_m (°C)	T_{d5} (°C)	λ_{abs} (nm)	μ_0 ($cm^2\ V^{-1}\ s^{-1}$)	E_g (eV)	I_P (eV)
V1422	148	276	430	293, 383, 468	9.86×10^{-7}	1.87	4.94
V1423	153	—	435	300, 383, 479	1.29×10^{-6}	1.90	4.94
V1454	175	307	445	285, 377, 467	3.38×10^{-6}	1.88	5.05
V1455	172	—	444	286, 377, 480	1.85×10^{-6}	1.89	5.08

V1454 and V1455 thin films are 1.87, 1.90, 1.88 and 1.89 eV, respectively (see Fig. 1c). The energy band diagram is presented in Fig. 1d and reveals agreeable band offsets conducive to the photogenerated carrier transport from the absorber to the metal back contact.

The Sb_2S_3 absorber layer was characterized using XRD and Raman spectroscopy. Data are presented in Fig. S4, in the ESI.† The XRD results confirmed the presence of a single phase of orthorhombic Sb_2S_3 (ICDD PDF 01-075-4013) without any secondary phase.[9,13,20,22] The Raman spectrum shows sharp peaks at 128, 155, 188, 236, 280, 302, and 312 cm^{-1}, which are characteristic of the crystalline Sb_2S_3 layer.[9,13,20,22] The band gap of the Sb_2S_3 film was 1.78 eV, as calculated from the absorption spectra using the Tauc plot (Fig. S4†), which is in line with the values previously reported for sprayed Sb_2S_3 films.[9,13,20,21] The SEM cross-sectional images of solar cells with two HTMs, V1423 and V1454, both deposited from 2 mM solutions, are presented in Fig. S5, in the ESI.† The thickness of the Sb_2S_3 absorber layer was approximately 80 nm.

To study a possible chemical interaction at the Sb_2S_3/HTM interface, XPS studies were performed for HTMs on a glass substrate and Sb_2S_3 solar cell stacks without and with an HTM. The XPS spectra of Sb_2S_3/HTM (V1422, V1423, V1454 and V1455) samples in the Sb 3d region and S 2p region are shown in the ESI, in Fig. S6 and S7,† respectively. The Sb 3d spectra for Sb_2S_3 films and Sb_2S_3 covered with a thin layer of V1423 and V1454, are shown in Fig. 2a and b, respectively. The binding energies (BEs) of Sb 3d core level peaks in the Sb_2S_3 sample are located at 539.7 eV for Sb $3d_{3/2}$ and 530.3 eV for Sb $3d_{5/2}$. For the samples of Sb_2S_3 with V1423, the BE peak positions are shifted to lower energy values, to 539.2 eV for Sb $3d_{3/2}$ and to 529.9 eV for Sb $3d_{5/2}$.

A similar shift in Sb 3d core level peak positions to lower BE values is also observed for the sample with V1454 as the HTM (Fig. 2b). The noted shift towards lower binding energy values, in comparison to pristine Sb_2S_3, indicates an increased electron density around the Sb atoms in the absorber. A similar shift in the Sb 3d core level peak was observed when a dithieno[3,2-*b*:20,30-*d*]pyrrole-cored small molecule (DTPThMe-ThTPA)[32] and thiophene-modified quinoxaline core small molecules[27] were applied onto the $Sb_2(S,Se)_3$ film.

S 2p core level spectra for Sb_2S_3 films, HTMs (V1423, V1454) and Sb_2S_3/HTM samples are shown in Fig. 2c and d. S $2p_{3/2}$ peaks for Sb_2S_3 and Sb_2S_3/V1423 samples are positioned at BEs of 162.0 and 161.5 eV, respectively (see Fig. 2c). A similar shift of the S $2p_{3/2}$ peak towards the lower BE region is observed when V1454 is applied onto Sb_2S_3 (Fig. 2d). V1454 deposited onto a glass substrate shows the S $2p_{3/2}$ peak at 162.4 eV, but after deposition of V1454 onto Sb_2S_3 the S 2p peak of V1454 shifted to a higher energy region and peaked at a BE of 164.2 eV (see Fig. 2d and Fig. S7 in the ESI†).

A similar shift of the S 2p peak of thiophene-modified quinoxaline core small molecules to higher energies has been detected when applied to the $Sb_2(S,Se)_3$ layer.[27] Interestingly, we did not detect S 2p peaks characteristic of V1423 in the spectrum of the Sb_2S_3/V1423 stack (Fig. 2c), although the shifts in the positions of S 2p peak and Sb 3d peak of the Sb_2S_3 were clearly detected upon application of V1423 onto Sb_2S_3. The

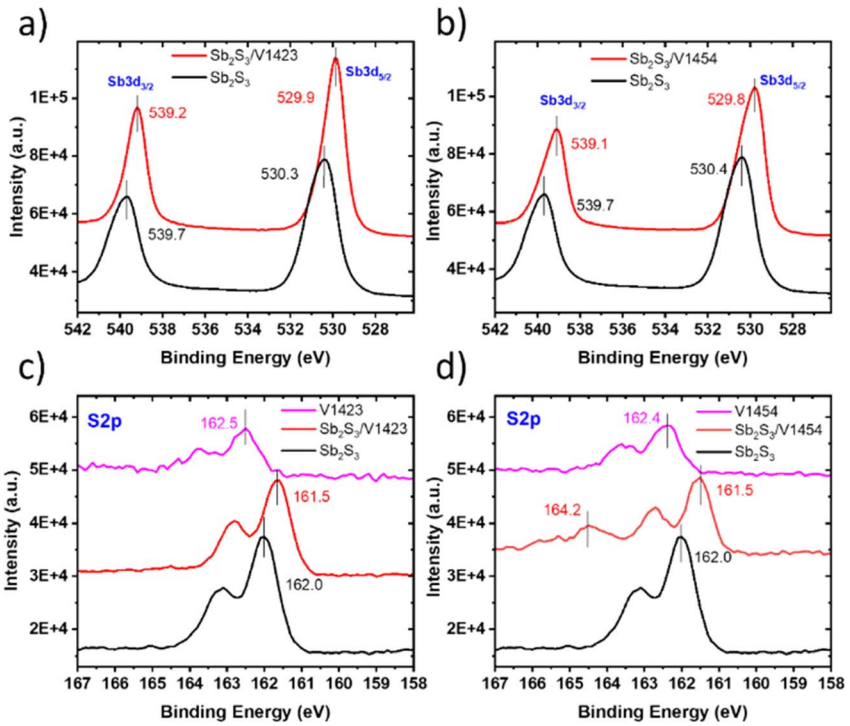

Fig. 2 XPS core level spectra (a) Sb 3d for Sb_2S_3 and Sb_2S_3/V1423, (b) Sb 3d for Sb_2S_3 and Sb_2S_3/V1454, (c) S 2p for Sb_2S_3, V1423 and Sb_2S_3/V1423, and (d) S 2p for Sb_2S_3, V1454 and Sb_2S_3/V1454.

shifts observed in Sb 3d and S 2p peak positions of Sb_2S_3 as well as in S 2p peak positions of HTMS refer to the interaction between S atoms from electron-rich thiophene units and Sb atoms from the Sb-chalcogenide compound which is expected to improve the interfacial carrier extraction ability.

Solar cells based on Sb_2S_3 were prepared in the superstrate configuration glass/FTO/TiO_2/Sb_2S_3/HTM/Au (see the sketch in Fig. 3a and SEM images in Fig. S5, in the ESI†). The systematic change in the concentration of V-series HTM solutions (4, 2, 1, 0.6 mM) was studied. The resulting output parameters are presented in Table S1, in the ESI.† Solar cells fabricated with 2 mM solutions showed the highest performance, independent of the HTM used. The current–voltage (J–V) characteristics of the best performing devices using 2 mM HTM solutions are presented in Fig. 3b, and the cell output parameters are summarized in Table 2. The reference device, lacking an HTM, yielded a V_{OC} of 478 mV, J_{SC} of 8.7 mA cm^{-2}, FF of 0.46, and a PCE of 1.9%. Introduction of V1422 and V1423 as HTMs resulted in open circuit voltages of 656 and 673 mV, respectively. On application of HTMs, also other solar cell parameters improved as compared to the cells without an HTM. In the case of the cell with V1423, J_{SC} improved from 9.0 to 12.1 mA cm^{-2}, FF from 0.46 to 0.56 and PCE from 1.9 to 4.5%. Therefore, the utilization of HTMs – V1422 and V1423 substantially mitigates carrier recombination at the back interface, leading to improved carrier collection. Notably, the device with the HTM – V1423 yielded device output characteristics comparable to those employing P3HT. In contrast, solar cell devices with V1454 and V1455, having triphenylamine side fragments, yielded V_{OC} values of 439 and 437 mV, respectively. As compared to the solar cell without any HTM, there was no improvement in V_{OC} values. In addition, an increase in series resistance (R_S) values and a decrease in J_{SC}, FF and overall PCE was recorded (Fig. 3b and Table 2). High R_S values up to *ca.* 5 Ω cm^2 in solar cells could result from an excessively thick layer. For the purpose of reducing the HTM layer thickness, solar cells were fabricated with diluted HTM solutions. The concentration of HTM solutions was decreased from 2 mM to 0.6 mM. However, no notable improvement in solar cell parameters was observed, as detailed in the ESI, Table S1.† The external quantum efficiency (EQE)

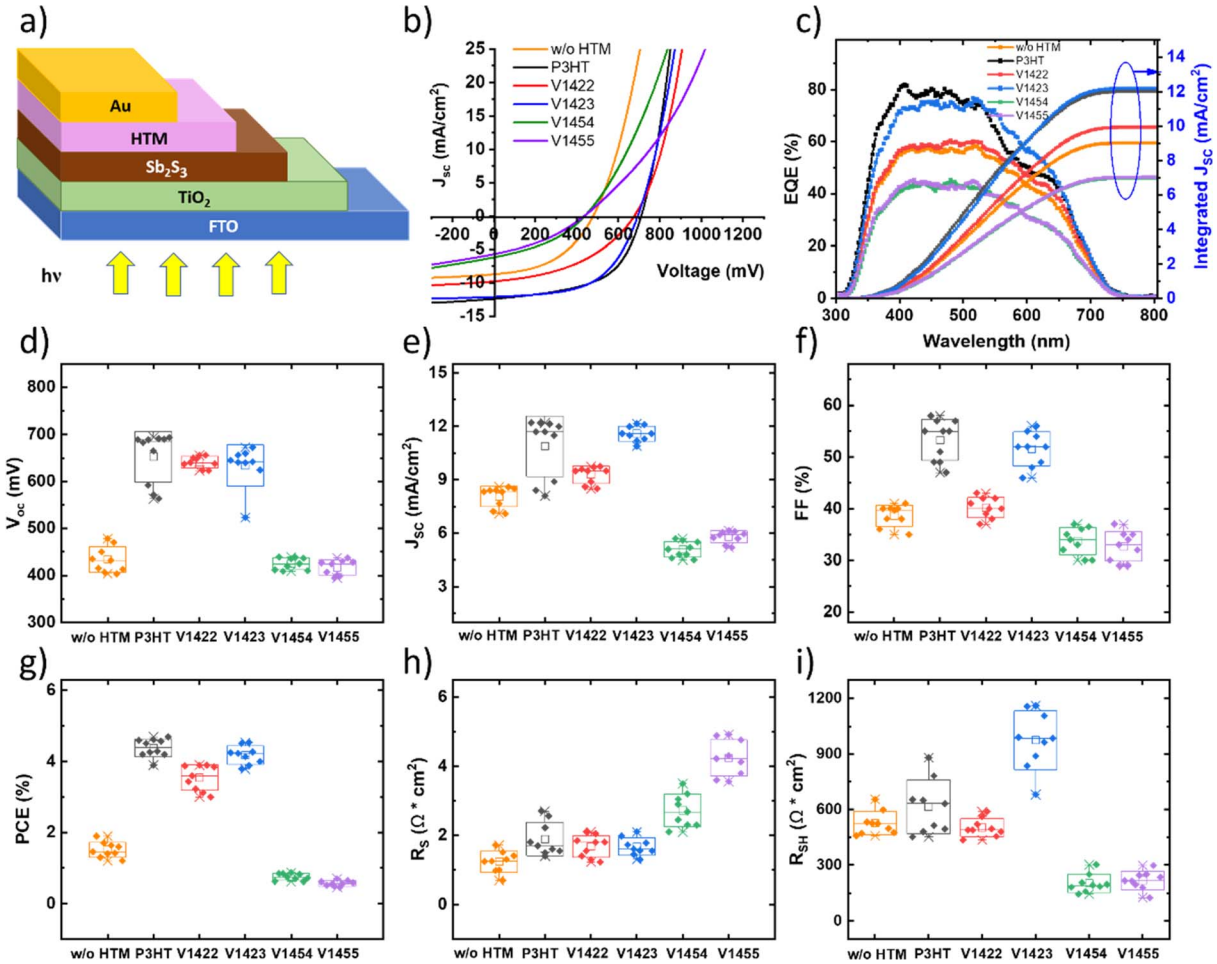

Fig. 3 (a) Schematic of the Sb_2S_3 absorber solar cell (glass/FTO/TiO_2/Sb_2S_3/HTM/Au) fabricated in the superstrate configuration, (b) J–V characteristics, (c) external quantum efficiency (EQE) curves with the calculated integrated J_{SC} curves of the champion solar cells without (w/o) the HTM and with different HTMs (P3HT, V1422, V1423, V1454 and V1455). Box plots of Sb_2S_3 solar cells without any HTM (Sb_2S_3/Au) and with P3HT, V1422, V1423, V1454 and V1455 as HTMs: (d) V_{OC}, (e) J_{SC}, (f) fill factor (FF), (g) PCE, (h) series resistance (R_S), and (i) shunt resistance (R_{SH}).

Table 2 Key performance metrics of champion Sb_2S_3 solar cells without (w/o) any HTM and with HTMs (V1422, V1423, V1454, V1455 and P3HT)

HTM	HTM conc. (mg mL^{-1})	V_{OC} (mV)	J_{SC} (mA cm^{-2})	Integrated J_{SC} (mA cm^{-2})	FF (%)	PCE (%)	R_S (Ω cm^2)	R_{SH} (Ω cm^2)
w/o	—	478	8.7	9.0	46	1.9	1.1	514
V1422	2 mM	656	9.7	9.9	43	3.9	1.7	436
V1423	2 mM	673	12.1	12.0	56	4.5	1.3	1005
V1454	2 mM	439	5.7	6.8	35	0.8	2.7	192
V1455	2 mM	437	6.1	7.1	33	0.7	4.9	198
P3HT	1 wt%	689	12.2	12.2	55	4.7	1.8	526

graphs of the champion devices without any HTM and with different HTM layers are presented in Fig. 3c. It should be noted that the integrated J_{SC}, calculated based on EQE spectra, closely correspond to the values obtained from the *J–V* curves (see Table 2). A dip in the spectral response in the case of the device with P3HT can be seen in the range of 550–650 nm, which is attributed to its parasitic absorption losses.[20,22] Normalized EQE curves of the devices with investigated HTMs are presented in the ESI, in Fig. S9.† The concavity in the EQE curve is less pronounced in the case of samples with V-series HTMs. All investigated HTMs have a similar band gap, within the range of 1.8–1.9 eV. However, the V-series HTM layers were considerably thinner, approximately 20–25 nm, in contrast to P3HT, with a thickness of about 80–100 nm. Thus, devices with V-series HTMs show an average visible transmittance (AVT) of 24–26% compared to 21% by the P3HT-based device (see Fig. S10 in the ESI†). A statistical representation (*i.e.*, box plots) of solar cell parameters of the fabricated cells without any HTM and with investigated HTMs (Fig. 3d–i) refers to high reproducibility of the results.

Although the interaction between the S atom from the thiophene unit and Sb from Sb_2S_3 has been noted in all interfaces with V-series HTMs, only the use of V1422 and V1423 as HTMs led to an increase in the open-circuit voltage (V_{OC}) of up to 650–670 mV. Furthermore, only the application of V1423 in the solar cell structure resulted in fill factor values of up to 56%, leading to conversion efficiencies exceeding 4% (see box-plot, in Fig. 3), which is very close to that obtained using P3HT as the HTM. Our results show that V1423, a dimer molecule with three thiophene units in its structure is the most efficient one in this family of novel HTMs. The application of V1454 and V1455 as HTM layers did not reduce the interface recombination or improve the carrier collection. V_{OC} remains on the level of 400 mV comparable to the cells without the HTM, fill factor values are low and vary in the region 30–35%. The current density is *ca.* two times lower as compared to the cell with V1423 and the solar cell exhibits a high R_S value of *ca.* 5 Ω cm^2 (Fig. 3d–i). Consequently, the solar cell conversion efficiencies are below 1%, that is two times lower than that recorded for the cells without any HTM.

As stated above, the interaction of S from the thiophene unit with Sb from Sb_2S_3 at the absorber surface may explain the improvement of the V_{OC} and overall solar cell parameters *via* passivation of the interfacial states. Although such a mechanism is validated by the enhanced V_{OC} in V1422 and V1423-based devices, the abrupt decrease in the V_{OC} and overall performance of V1454 and V1455-based cells indicate that there might be another concomitant phenomenon which prevails or compensates the benefit of thiophene-based interactions. A possible explanation for the low V_{OC} and PCE of V1454 and V1455-based cells, can be linked to the dipole effects at the absorber/HTM interface. As demonstrated in organic solar cells, insertion of organic materials between the photoactive absorber layer and electrodes can be an efficient approach for manipulation of the electric potential distribution by dipole moments at the electrode surface.[33–35] Several experimental and numerical simulation studies reported that the dipoles at the back/front interfaces have to be aligned in such a way that it allows accumulation of high hole concentration at the vicinity of hole contact and high electron density at the vicinity of electron contact.[33,36] The efficiency of photogenerated charge carrier separation (and thus, improved charge selectivity) is influenced by the specific arrangement of the molecules and the orientation of the permanent dipole moment. Thus, in some cases, depending on the angular configuration and molecular arrangement, the organic molecules can act as hole or electron selective layers. For example, Kippelen *et al.*, demonstrated that the HTM – PEDOT:PSS can be easily altered to a well-functionalized electron transport layer by complexation with polyethylenimine ethoxylated (PEIE) molecules.[37]

Considering these approaches, it can be assumed that in V1454 and V1455 based solar cell devices, the additional phenyl fragment in the HTMs reconfigured the angular and molecular arrangement resulting in unsuitable alignment in the orientation of the dipoles at the back interface. As a consequence, this imposes an increase of an "incorrect" type of charge carrier concentration in the vicinity of the metal back contact (*i.e.*, electron proximity of the Hall contact), decreasing the V_{OC} and deteriorating the overall device performance. Validation of this hypothesis can be assured by in-depth analysis of the changes in the work function of the contact electrode in proximity of the HTM. This approach would imply complex correlative measurements of Kelvin-probe AFM and UPS combined with numerical simulations which has been applied in organic solar cells[33] and remains a great challenge for the emerging Sb_2S_3/HTM interface.

The anomalous low performance of V1454 and V1455-based cells can be approached from a different angle – by analysing the molecular geometry and orbitals and correspondingly, the positions of the Highest Occupied Molecular Orbital (HOMO)

and Lowest Unoccupied Molecular Orbital (LUMO) of V1422 (a representative of molecules with diphenylamine units in their structures) and V1454 (a representative of molecules with triphenylamine units in their structures) from quantum chemical simulation. Fig. 4 presents the optimized geometry of HTM compound molecules of V1422 and V1454, and their HOMO and LUMO.

The result of the simulation shows that HOMO levels of both V1454 and V1422 are formed by fluorene and benzene rings, while LUMO is primarily located on the thiophene groups. In addition to this HOMO–LUMO configuration, compared to V1422 (having a nonplanar orientation of fluorene in relation to the thiophene groups), V1454 exhibits more planar arrangement of fluorene groups relative to the thiophene groups. The latter effect allows a greater accessibility of the thiophene moieties in V1454 and consequently, a stronger interaction between S atoms in the thiophene group and Sb from Sb_2S_3. This strong interaction is highlighted by the observed shift of the V1454 S $2p_{3/2}$ peak towards the higher BE region when applied onto Sb_2S_3 (Fig. 2d, XPS analysis). However, this strong interaction does not result in an improved charge carrier transport through the interface since the HOMO level is not located on thiophene moieties and thus the condition for the accumulation of the "right" type of charge carrier (*i.e.*, holes) at the back interface is not satisfied. Thus, the quantum chemical simulation results suggest that to achieve

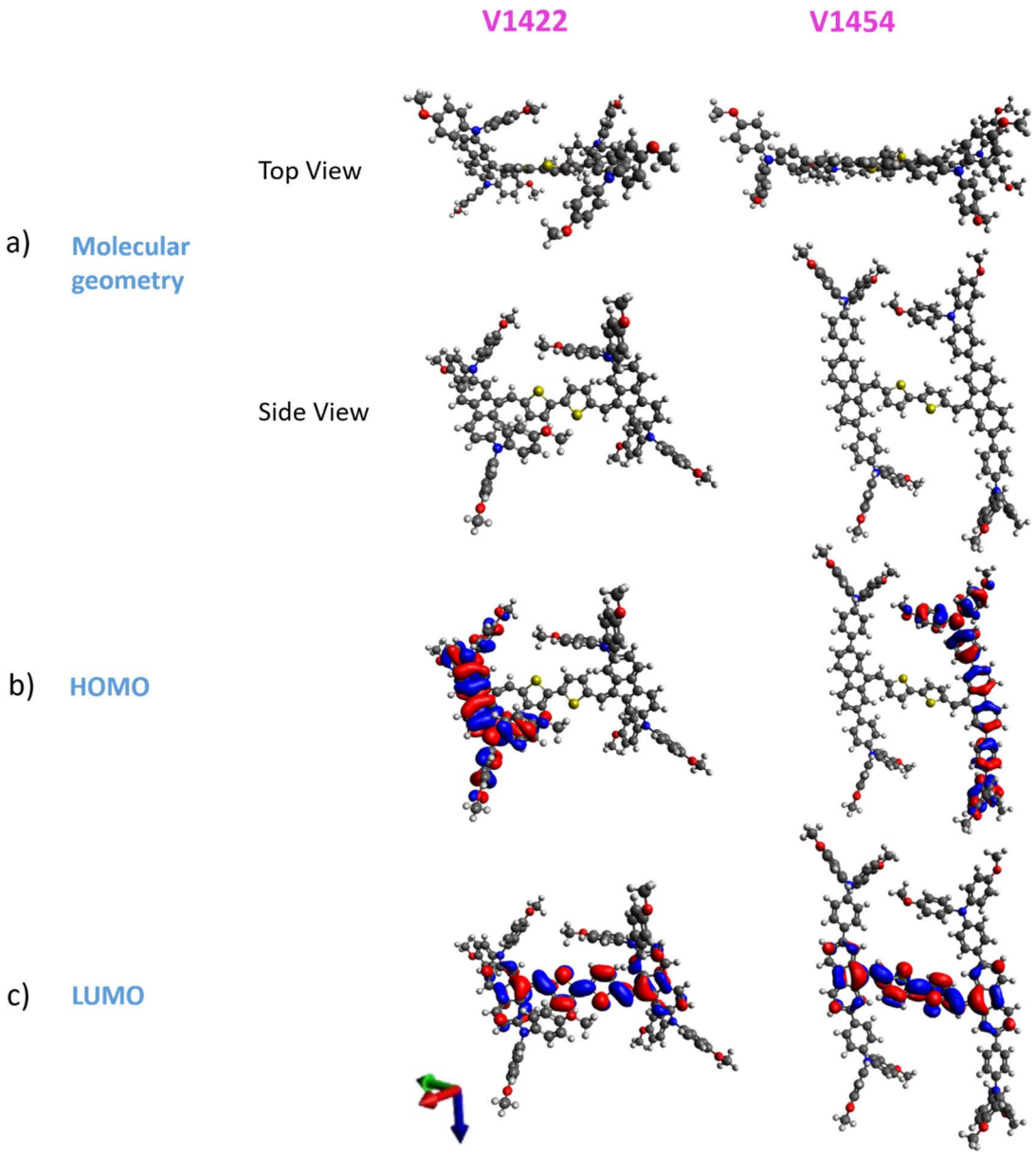

Fig. 4 (a) Optimized geometry of HTM molecules – V1422 and V1454 in top and side views, (b) highest occupied molecular orbital (HOMO) in HTMs – V1422 (left) and V1454 (right), (c) lowest unoccupied molecular orbital (LUMO) in HTMs – V1422 (left) and V1454 (right). Colors used for atoms: gray – C, white – H, yellow – S, red – O and blue – N.

higher efficiency of photogenerated charge carrier separation and improved charge selectivity by an organic HTM layer, the HOMO of the HTMs should be formed by the thiophene groups. Although this hypothesis may interfere with other requirements for the alignment of the electronic states at the organic/inorganic interfaces, these results lay a solid foundation for further investigations and understanding the charge transfer kinetics at the Sb_2S_3/HTM interface.

4. Conclusion

Four dopant-free dimers (V1422, V1423, V1454, V1455) comprising methoxydiphenylamine substituted fluorene derivatives and connected by central cores consisting of different numbers of thiophene moieties were synthesized by a solution chemical route. Synthesized organic semiconductors are molecular glasses, exhibiting glass transition and thermal decomposition temperatures of 148–175 °C and 430–445 °C, respectively and having an energy band gap of 1.9 eV and ionization potential of 4.9–5.1 eV. Synthesized organic semiconductors were explored, for the first time, as HTMs in superstrate configuration FTO/TiO_2/Sb_2S_3/HTM/Au solar cells in which the Sb_2S_3 absorber and TiO_2 layers were deposited by the ultrasonic spray method while HTM layers were obtained by spin-coating. Energy level diagrams demonstrate agreeable band offsets validating the applicability of the synthesized materials as efficient HTMs in an FTO/TiO_2/Sb_2S_3/HTM/Au device. It has been shown that application of the HTM layer on top of the Sb_2S_3 layer induces a shift in the Sb 3d core level peak to lower binding energies, indicating increased electron density surrounding the Sb atoms. Such a shift confirms the interaction between S atoms from thiophene units and Sb atoms from the absorber occurring at the Sb_2S_3/HTM interface. By introducing HTMs comprising diphenylamine units in their structures (V1422, V1423) into the solar cell structure, an increase in the device output characteristics compared to the device without an HTM layer was observed. The highest boost in device performance was observed for V1423-based cells, exhibiting an increase of the V_{OC} from 478 mV to 673 mV, fill factor from 46% to 56%, and PCE from 1.9% to 4.5%.

Thus, it can be concluded that this type of HTM effectively mitigates carrier recombination at the back interface, and contributes to better collection of carriers. The application of V1454 and V1455 (molecules with triphenylamine units in their structures) as HTM layers did not improve the device parameters as the V_{OC} remained on the level of 430 mV (comparable to the cells without HTMs) while the fill factor values reached the lowest level of 30–35%. For the same cells, the J_{SC} values were two times lower compared to the cells with V1423 and the PCEs of solar cells were below 1% – two times lower than those recorded for the cells without any HTM. The abrupt decrease in the V_{OC}, J_{SC} and overall performance of V1454 and V1455-based cells indicates the presence of a concomitant phenomenon which prevails or compensates the benefit of thiophene-based interactions. Possible phenomena occurring at the Sb_2S_3/HTM interface were discussed through the prism of correlation between the efficiency of the charge transfer/charger selectivity and final device performance, including possible impacts of the dipole effect as well as a prospective analysis from the quantum chemical simulation side. The results of quantum chemical simulation suggest that to achieve higher efficiency of photogenerated charge carrier separation and improved charge selectivity by the organic HTM layer, the HOMO of the HTMs should be configured by the thiophene groups. So far, the results of this study provide new perspectives on the chemical and physical understanding of Sb_2S_3/HTM organic/inorganic interfaces towards the identification of suitable innovative HTMs which would allow a significant boost in the efficiency of the emerging Sb-chalcogenide thin film PV technology.

Data availability

The data that support the findings of this study will be made available by the corresponding author upon request.

Author contributions

Nimish Juneja – conceptualization, methodology, validation, data curation, writing – original draft. Aistė Jegorovė – conceptualization, methodology, validation, writing – review & editing. Raitis Grzibovskis – methodology, validation, writing – review & editing. Atanas Katerski – methodology, validation. Maryte Daskeviciene – writing – review & editing. Tadas Malinauskas – writing – review & editing. Aivars Vembris – conceptualization, methodology, validation, writing – review & editing. Smagul Karazhanov – writing – review & editing. Nicolae Spalatu – methodology, formal analysis, visualization, supervision, writing – review & editing. Vytautas Getautis – conceptualization, methodology, validation, writing – review & editing. Malle Krunks – conceptualization, methodology, validation, supervision, writing – review & editing. Ilona Oja Acik – conceptualization, funding acquisition, project administration, writing – review & editing.

Conflicts of interest

There are no conflicts to declare.

Acknowledgements

The "Development of Semi-Transparent Bifacial Thin Film Solar Cells for Innovative Applications" benefits from a 999372 € grant from Iceland, Liechtenstein and Norway through the EEA Grants. The aim of the project is to develop a new approach based on novel materials and structures and production technologies, which are the key to further increasing the share, and range of application of PV in areas with sub-average sunlight, including Baltic and Nordic countries. Therefore, development of resource saving, cost-effective and efficient PV devices is a primary challenge of this project. The project contract no. with the Research Council of Lithuania (LMTLT) is S-BMT-21-1 (LT08-2-LMT-K-01-003). Department of Materials and Environmental Technology, Tallinn University of Technology has received funding from the Estonian Research Council, projects

PRG627 "Antimony Chalcogenide Thin films for Next-Generation Semi-transparent Solar Cells Applicable in Electricity Producing Windows" and PSG689 "Bismuth Chalcogenide Thin-Film Disruptive Green Solar Technology for Next Generation Photovoltaics". The research was partially funded by the European Union's Horizon 2020 ERA Chair project 5GSOLAR (grant agreement no. 952509). The research was supported by the European Cooperation in Science and Technology (COST) project RENEW-PV (CA21148) and by the Estonian Ministry of Education and Research (project TK210; TK210U8 "Center of Excellence in Sustainable Green Hydrogen and Energy Technologies"). Institute of Solid-State Physics, University of Latvia has received funding from the European Union's Horizon 2020 Framework Programme H2020-WIDESPREAD-01-2016-2017-TeamingPhase2 under grant agreement no. 739508, project CAMART^2.

Notes and references

1 N. Cates and M. Bernechea, *APL Mater.*, 2018, **6**, 084503.
2 S. Barthwal, R. Kumar and S. Pathak, *ACS Appl. Energy Mater.*, 2022, **5**, 6545–6585.
3 M. Koltsov, S. V. Gopi, T. Raadik, J. Krustok, R. Josepson, R. Gržibovskis, A. Vembris and N. Spalatu, *Sol. Energy Mater. Sol. Cells*, 2023, **254**, 112292.
4 C. Comparotto, P. Ström, O. Donzel-Gargand, T. Kubart and J. J. S. Scragg, *ACS Appl. Energy Mater.*, 2022, **5**, 6335–6343.
5 S. Wang, Y. Zhao, B. Che, C. Li, X. Chen, R. Tang, J. Gong, X. Wang, G. Chen, T. Chen, J. Li and X. Xiao, *Adv. Mater.*, 2022, **34**, 2206242.
6 Y. Zhao, S. Wang, C. Li, B. Che, X. Chen, H. Chen, R. Tang, X. Wang, G. Chen, T. Wang, J. Gong, T. Chen, X. Xiao and J. Li, *Energy Environ. Sci.*, 2022, **15**, 5118–5128.
7 Y. Zhao, S. Wang, C. Jiang, C. Li, P. Xiao, R. Tang, J. Gong, G. Chen, T. Chen, J. Li and X. Xiao, *Adv. Energy Mater.*, 2022, **12**, 2103015.
8 A. A. F. Husain, W. Z. W. Hasan, S. Shafie, M. N. Hamidon and S. S. Pandey, *Renewable Sustainable Energy Rev.*, 2018, **94**, 779–791.
9 J. S. Eensalu, A. Katerski, E. Kärber, L. Weinhardt, M. Blum, C. Heske, W. Yang, I. Oja Acik and M. Krunks, *Beilstein J. Nanotechnol.*, 2019, **10**, 2396–2409.
10 V. K. H. Bui and T. P. Nguyen, *Polymers*, 2023, **15**, 4443.
11 E. Zimmermann, T. Pfadler, J. Kalb, J. A. Dorman, D. Sommer, G. Hahn, J. Weickert and L. Schmidt-Mende, *Adv. Sci.*, 2015, **2**, 1500059.
12 M. S. You, C.-S. Lim, D. H. Kwon, J. H. Heo, S. H. Im and K. J. Chae, *Org. Electron.*, 2015, **21**, 155–159.
13 J. S. Eensalu, A. Katerski, E. Kärber, I. Oja Acik, A. Mere and M. Krunks, *Beilstein J. Nanotechnol.*, 2019, **10**, 198–210.
14 J. Chen, J. Qi, R. Liu, X. Zhu, Z. Wan, Q. Zhao, S. Tao, C. Dong, G. Y. Ashebir, W. Chen, R. Peng, F. Zhang, S. Yang, X. Tian and M. Wang, *Commun. Chem.*, 2019, **2**, 121.
15 Y. Zhang, S. Li, R. Tang, X. Wang, C. Chen, W. Lian, C. Zhu and T. Chen, *Energy Technol.*, 2018, **6**, 2126–2131.
16 Y. Yang, C. Shi, K. Lv, Q. Wang, X. Sun and W. Chen, *New J. Chem.*, 2021, **45**, 10357–10361.
17 X. Jin, Y. Fang, T. Salim, M. Feng, Z. Yuan, S. Hadke, T. C. Sum and L. H. Wong, *Adv. Mater.*, 2021, **33**, 2104346.
18 R. Tang, X. Wang, W. Lian, J. Huang, Q. Wei, M. Huang, Y. Yin, C. Jiang, S. Yang, G. Xing, S. Chen, C. Zhu, X. Hao, M. A. Green and T. Chen, *Nat. Energy*, 2020, **5**, 587–595.
19 M. L. Petrus, T. Bein, T. J. Dingemans and P. Docampo, *J. Mater. Chem. A*, 2015, **3**, 12159–12162.
20 N. Juneja, S. Mandati, A. Katerski, N. Spalatu, S. Daskeviciute-Geguziene, A. Vembris, S. Karazhanov, V. Getautis, M. Krunks and I. Oja Acik, *Sustainable Energy Fuels*, 2022, **6**, 3220–3229.
21 N. Juneja, S. Daskeviciute-Geguziene, N. Spalatu, S. Mandati, A. Katerski, R. Grzibovskis, A. Vembris, S. Karazhanov, V. Getautis, M. Krunks and I. Oja Acik, *Mater. Sci. Semicond. Process.*, 2024, **169**, 107934.
22 S. Mandati, N. Juneja, A. Katerski, A. Jegorovė, R. Grzibovskis, A. Vembris, T. Dedova, N. Spalatu, A. Magomedov, S. Karazhanov, V. Getautis, M. Krunks and I. Oja Acik, *ACS Appl. Energy Mater.*, 2023, **6**, 3822–3833.
23 D. Poplavskyy and J. Nelson, *J. Appl. Phys.*, 2003, **93**, 341–346.
24 S.-J. Moon, Y. Itzhaik, J.-H. Yum, S. M. Zakeeruddin, G. Hodes and M. Grätzel, *J. Phys. Chem. Lett.*, 2010, **1**, 1524–1527.
25 S. Daskeviciute, C. Momblona, K. Rakstys, A. A. Sutanto, M. Daskeviciene, V. Jankauskas, A. Gruodis, G. Bubniene, V. Getautis and M. K. Nazeeruddin, *J. Mater. Chem. A*, 2021, **9**, 301–309.
26 T. Malinauskas, D. Tomkute-Luksiene, R. Sens, M. Daskeviciene, R. Send, H. Wonneberger, V. Jankauskas, I. Bruder and V. Getautis, *ACS Appl. Mater. Interfaces*, 2015, **7**, 11107–11116.
27 Y. Xiang, H. Guo, Z. Cai, C. Jiang, C. Zhu, Y. Wu, W.-H. Zhu and T. Chen, *Chem. Commun.*, 2022, **58**, 4787–4790.
28 S. Xu, J. Wu, F. Guo, M. Wu, S. Chen, W. Chen and C. Shi, *Sustainable Energy Fuels*, 2023, **7**, 61–65.
29 S. H. Im, C.-S. Lim, J. A. Chang, Y. H. Lee, N. Maiti, H.-J. Kim, M. K. Nazeeruddin, M. Grätzel and S. Il Seok, *Nano Lett.*, 2011, **11**, 4789–4793.
30 M. J. Frisch, G. W. Trucks, H. B. Schlegel, G. E. Scuseria, M. A. Robb, J. R. Cheeseman, G. Scalmani, V. Barone, G. A. Petersson and H. Nakatsuji, *Gaussian 09, Revision A.02*, Gaussian Inc., Wallingford CT, 2016.
31 M. V. Khenkin, E. A. Katz, A. Abate, G. Bardizza, J. J. Berry, C. Brabec, F. Brunetti, V. Bulović, Q. Burlingame, A. Di Carlo, R. Cheacharoen, Y.-B. Cheng, A. Colsmann, S. Cros, K. Domanski, M. Dusza, C. J. Fell, S. R. Forrest, Y. Galagan, D. Di Girolamo, M. Grätzel, A. Hagfeldt, E. von Hauff, H. Hoppe, J. Kettle, H. Köbler, M. S. Leite, S. Liu, Y.-L. Loo, J. M. Luther, C.-Q. Ma, M. Madsen, M. Manceau, M. Matheron, M. McGehee, R. Meitzner, M. K. Nazeeruddin, A. F. Nogueira, Ç. Odabaşı, A. Osherov, N.-G. Park, M. O. Reese, F. De Rossi, M. Saliba, U. S. Schubert, H. J. Snaith, S. D. Stranks, W. Tress, P. A. Troshin, V. Turkovic, S. Veenstra, I. Visoly-Fisher, A. Walsh, T. Watson, H. Xie, R. Yıldırım, S. M. Zakeeruddin, K. Zhu and M. Lira-Cantu, *Nat. Energy*, 2020, **5**, 35–49.

32 C. Jiang, J. Zhou, R. Tang, W. Lian, X. Wang, X. Lei, H. Zeng, C. Zhu, W. Tang and T. Chen, *Energy Environ. Sci.*, 2021, **14**, 359–364.
33 U. Würfel, M. Seßler, M. Unmüssig, N. Hofmann, M. List, E. Mankel, T. Mayer, G. Reiter, J. Bubendorff, L. Simon and M. Kohlstädt, *Adv. Energy Mater.*, 2016, 1600594.
34 J. Kesters, T. Ghoos, H. Penxten, J. Drijkoningen, T. Vangerven, D. M. Lyons, B. Verreet, T. Aernouts, L. Lutsen, D. Vanderzande, J. Manca and W. Maes, *Adv. Energy Mater.*, 2013, **3**, 1180–1185.
35 F. A. Nüesch, *Chimia*, 2013, **67**, 388–392.
36 C. F. N. Marchiori and M. Koehler, *J. Phys. D Appl. Phys.*, 2014, **47**, 215104.
37 Y. Zhou, C. Fuentes-Hernandez, J. Shim, J. Meyer, A. J. Giordano, H. Li, P. Winget, T. Papadopoulos, H. Cheun, J. Kim, M. Fenoll, A. Dindar, W. Haske, E. Najafabadi, T. M. Khan, H. Sojoudi, S. Barlow, S. Graham, J.-L. Brédas, S. R. Marder, A. Kahn and B. Kippelen, *Science*, 2012, **336**, 327–332.

